# Computational Elucidation of the Transition State Shape Selectivity Phenomenon

Louis A. Clark,* Marek Sierka,† and Joachim Sauer*

*Contribution from the Institut für Chemie, Humboldt-Universität zu Berlin, Unter den Linden 6, D-10099 Berlin, Germany*

Received August 28, 2003; E-mail: lc@chemie.hu-berlin.de; js@chemie.hu-berlin.de

**Abstract:** The most commonly cited example of a transition state shape selective reaction, *m*-xylene disproportionation in zeolites, is examined to determine if the local spatial environment of a reaction can significantly alter selectivity. In the studied reaction, ZPE-corrected rate limiting energy barriers are 136 kJ/mol for the methoxide-mediated pathway and 109 to 145 kJ/mol for the diphenylmethane-mediated pathway. Both pathways are likely to contribute to selectivity and disfavor one product isomer (1,3,5-trimethylbenzene), but relative selectivity to the other two isomers varies with pore geometry, mechanistic pathway, and inclusion of entropic effects. Most importantly, study of one pathway in three different common zeolite framework types (FAU, MFI, and MOR) allows explicit and practically oriented consideration of pore shape. Variation of the environment shape at the critical transition states is thus shown to affect the course of reaction. Barrier height shifts on the order of 10−20 kJ/mol are achievable. Observed selectivities do not agree with the transition state characteristics calculated here and, hence, are most likely due to product shape selectivity. Further examination of the pathways highlights the importance of mechanistic steps that do not result in isomer-defining bonds and leads to a more robust definition of transition state shape selectivity.

## 1. Introduction

The extent to which geometric constrictions influence the course of a catalytic reaction has long been open to speculation. Is it possible to control selectivity by designing the local spatial environment of a reaction? This work focuses on zeolites, but the concepts are applicable to a wide range of catalysts. One theory holds that enzymes enhance their activity by "steering" reactants into orbitally favored orientations.[1] Similarly, successful homogeneous chiral catalysts are thought to function by spatially controlling reactant encounters.[2] Zeolites have been used to encapsulate such chiral catalysts and improve selectivities through little-understood mechanisms.[3−8] Heterogeneous catalyst engineers have long sought to use the wide variety of zeolite pore shapes to control reaction selectivity.[9−12] Here we seek to add basic mechanistic understanding to shape confinement during reaction through the use of new computational tools.

Of the several mechanisms whereby pore shape can influence chemical reactions, the focus here is on local effects. The term "restricted transition state shape selectivity" was created to assert that local zeolite pore shape could alter the course of a reaction.[13,14] Initially it was invented to apply to the reaction of methyl-ethylbenzenes over mordenite zeolites.[13,15] The clearest definition simply states that "..certain reactions are prevented because the transition state is too large for the cavities of the molecular sieve".[14] As will be shown, there is a lack of experimental evidence for this phenomenon, and the concept is insufficiently defined. Computational work has demonstrated that selectivity-determining transition state structures are changed when the full zeolite environment is included, but only one pore type was studied and entropic effects have not be included.[16,17] A novel method incorporating entropic effects but using less reliable calculations showed that significant selectivity differences can result from simply changing the accessibility to the transition states.[18] It is not necessary to block reaction pathways to produce local selectivity changes, as the original definition suggested.

† Present address: Institut für Physikalische Chemie, Lehrstuhl für Theoretische Chemie, Universität Karlsruhe (TH), Kaiserstr. 12, D-76128 Karlsruhe, Germany.

(1) Mesecar, A. D.; Stoddard, B. L.; Koshland, D. E. *Science* **1997**, *277*, 202−206.
(2) Yoon, T. P.; Jacobsen, E. N. *Science* **2003**, *299*, 1691−1693.
(3) Leibovitch, M.; Olovsson, G.; Sundarababu, G.; Ramamurthy, V.; Scheffer, J. R.; Trotter, J. *J. Am. Chem. Soc.* **1996**, *118*, 1219−1220.
(4) Ogunwumi, S. B.; Bein, T. *Chem. Commun.* **1997**, 901−902.
(5) Joy, A.; Uppili, S.; Netherton, M. R.; Scheffer, J. R.; Ramamurthy, V. *J. Am. Chem. Soc.* **2000**, *122*, 728−729.
(6) Hutchings, G. J.; Willock, D. J. *Top. Catal.* **1998**, *5*, 177−185.
(7) Bein, T. *Curr. Opin. Solid State Mater. Sci.* **1999**, *4*, 85−96.
(8) Brunet, E. *Chirality* **2002**, *14*, 135−143.
(9) Csicsery, S. M. In *Zeolite Chemistry and Catalysis*; Rabo, J. A., Ed.; American Chemical Society: Washington, DC, 1976; Vol. 171, pp 680−718.
(10) Chen, N. Y.; Degnan, T. F., Jr.; Smith, C. M. *Molecular Transport and Reaction in Zeolites*; VCH Publishers: New York, 1994.
(11) Song, C.; Garces, J. M.; Sugi, Y., Eds. *Shape-Selective Catalysis*; ACS Symposium Series 738; American Chemical Society: Washington, DC, 2000.

(12) Mohanty, S.; McCormick, A. V. *Chem. Eng. J. (Lausanne)* **1999**, *74*, 1−2.
(13) Csicsery, S. M. *J. Catal.* **1971**, *23*, 124−130.
(14) Csicsery, S. M. *Zeolites* **1984**, *4*, 202−213.
(15) Csicsery, S. M. *J. Catal.* **1987**, *108*, 433−443.
(16) Vos, A. M.; Rozanska, X.; Schoonheydt, R. A.; Santen, R. A. V.; Hutschka, F.; Hafner, J. *J. Am. Chem. Soc.* **2001**, *123*, 2799−2809.
(17) Rozanska, X.; Santen, R. A. V.; Hutschka, F.; Hafner, J. *J. Am. Chem. Soc.* **2001**, *123*, 7655−7667.
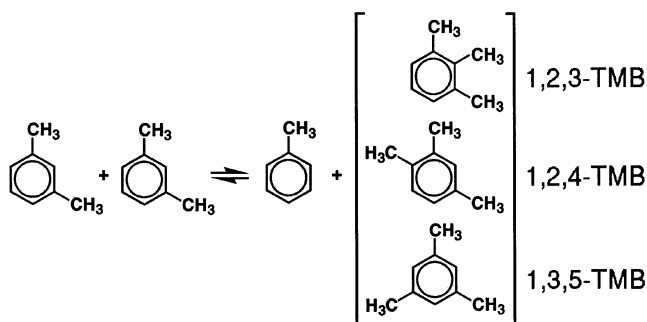
**Figure 1.** Reactants and final products of the *m*-xylene disproportionation reaction.

A unifying perspective of local pore shape effects on reaction selectivity is needed. Preferably, it should be based on the classical picture of intermediates and transition states on a potential energy surface. In light of the experimental difficulties involved in examining local environmental effects during reaction, a theoretical approach to the study of transition state shape selectivity seems warranted and is perhaps the only choice. Computational methodologies for studying shape selectivity vary widely and are still being actively developed. In this work, we examine potential energy surfaces using a newly available mixed quantum mechanical−molecular mechanical (QM/MM) technique.[19] The results allow us to give a useful decomposition of local pore shape effects into the importance of relative intermediate stabilities and into the transition state barrier heights throughout the reaction pathway. Explicit calculations of reaction barriers in different pore geometries will be made to ascertain how much the local environmental shape affects the transition states. Only very recently, such results became available, albeit for a sterically less demanding reaction, the chemisorption of isobutene.[20]

In this work, the disproportionation of *m*-xylene is chosen because it is the most studied potential transition state shape selectivity reaction. As an aromatic transformation reaction, it is also very important industrially.[21] Transfer of a methyl group from one *m*-xylene to another leads to toluene and three possible trimethylbenzene (TMB) isomers as shown in Figure 1. Martens et al. used pencil-and-paper fitting arguments to suggest that the trimethylbenzene product distribution of this reaction is controlled by pore shape.[22] Since this work, the reaction has often been used as a test to characterize zeolite pores.[23−29]

**1.1. Absence of Experimental Evidence.** There is little doubt that global zeolite pore shape can control the course of a reaction. *Reactant shape selectivity* refers to the selectivity produced when larger molecules cannot enter the zeolite pores and reach most of the active sites.[30] In *product shape selectivity*, pore constrictions severely curtail diffusion of the bulkiest products. More slowly diffusing products isomerize to their faster cousins and escape the pores as observable species. The effect is inherently powerful, because isomer diffusivity can vary by orders of magnitude. Industrial production of *para*-xylene over modified ZSM-5 catalysts is the pervasive example of product shape selectivity.[10] In support of the concept, passivation of the nonshape selective external surface[31,32] and increases in the crystal size both lead to selection of the faster-diffusing product. Differences between NMR measurements of product concentrations inside and gas chromatography measurements outside pores also support this concept,[33] as does analytical modeling.[34]

In constrast, *there is no experimental evidence for transition state shape selectivity*. It is often invoked loosely to explain reaction selectivities,[22,35−37] but attribution to the necessarily local effect is experimentally difficult. Distinguishing between product and transition state shape selectivity is particularly difficult. Since the product shape selectivity effect is dependent on diffusion, if the size of the zeolite crystal is varied, the reaction selectivity should change.[38] In practice, this test is almost never performed because preparing the necessary series of catalysts is difficult. In the rare cases where it has been tested on aromatic reactions, product composition typically changes with crystallite size, indicating that, at a minimum, product shape selectivity is operative.[39−41]

Since the initial conception of the idea, researchers have sought to modify the concepts of local shape selectivity effects to explain their experimental results. Anderson and Klinowski's interpreted their MAS NMR spectra to indicate that the proportions of tetramethylbenzenes inside their HZSM-5 catalyst was significantly different from the equilibrium distribution.[42] They believed that the spatial active site environment was restricting isomerization and proposed that a new type of shape selectivity, "active site shape selectivity", was operative. Santilli et al. coined the term "inverse shape selectivity" after their computations showed that branched hexanes should be favored in certain pore structures over their linear counterparts because they fit better.[43] The more highly branched molecule concentrations inside the pores then similarly influence the external product distribution. Both of these effects are based on altering the equilibrium distribution of isomers inside the pores.

(18) Clark, L. A.; Snurr, R. Q. In *Zeolite and Mesoporous Materials at the Dawn of the 21st Century*; Galarneau, A., Renzo, F. D., Fajula, F., Vedrine, J., Eds.; Elsevier: Amsterdam, 2001; Vol. 138 of *Studies in Surface Science and Catalysis*, CD indexed by title or author name.
(19) Sierka, M.; Sauer, J. *J. Chem. Phys.* **2000**, *112*, 6983−6996.
(20) Rozanska, X.; Van Santen, R. A.; Demuth, T.; Hutschka, F.; Hafner, J. *J. Phys. Chem. B* **2003**, *107*, 1309−1315.
(21) Tsai, T. C.; Liu, S. B.; Wang, I. *Appl. Catal. A* **1999**, *181*, 355−398.
(22) Martens, J. A.; Perez-Pariente, J.; Sastre, E.; Corma, A.; Jacobs, P. A. *Appl. Catal.* **1988**, *45*, 85−101.
(23) Pérez-Pariente, J.; Sastre, E.; Fornés, V.; Martens, J. A.; Jacobs, P. A.; Corma, A. *Appl. Catal.* **1991**, *69*, 125−137.
(24) Weitkamp, J.; Ernst, S. *Catal. Today* **1994**, *19*, 107−150.
(25) Adair, B.; Chen, C. Y.; Wan, K. T.; Davis, M. E. *Microporous Mater.* **1996**, *7*, 261−270.
(26) Morin, S.; Ayrault, P.; El Mouahid, S.; Gnep, N. S.; Guisnet, M. *Appl. Catal.* **1997**, *159*, 317−331.
(27) Jones, C. W.; Zones, S. I.; Davis, M. E. *Appl. Catal.* **1999**, *181*, 289−303.
(28) Jones, C. W.; Zones, S. I.; Davis, M. E. *Microporous Mesoporous Mater.* **1999**, *28*, 471−481.
(29) Corma, A.; Chica, A.; Guil, J. M.; Llopis, F. J.; Mabilon, G.; Perdigon-Melon, J. A.; Valencia, S. *J. Catal.* **2000**, *189*, 382−394.

(30) Weisz, P. B.; Frilette, V. J. *J. Phys. Chem.* **1960**, *64*, 382.
(31) Chen, N. Y.; Kaeding, W. W.; Dwyer, F. G. *J. Am. Chem. Soc.* **1979**, *101*, 6783−6784.
(32) Hibino, T.; Niwa, M.; Murakami, Y. *J. Catal.* **1991**, *128*, 551−558.
(33) Anderson, M. W.; Klinowski, J. *Nature* **1989**, *339*, 200−203.
(34) Wei, J. *J. Catal.* **1982**, *76*, 433−439.
(35) Hölderich, W. F. In *Guidelines for Mastering the Properties of Molecular Sieves*; Barthomeuf, E. D., Hölderich, W., Eds.; Plenum Press: London, 1990; Vol. NATO ASI Series, B, Physics-Vol. 221, pp 319−342.
(36) Mirth, G.; Čejka, J.; Nusterer, E.; Lercher, J. A. In *Zeolites and Microporous Crystals*; Hattori, T., Yashima, T., Eds.; Elsevier: 1994; Vol. 83 of *Studies in Surface Science and Catalysis*, pp 287−294.
(37) Wichterlova, B.; Cejka, J.; Zilková, J. *Microporous Mater.* **1996**, *6*, 405−414.
(38) Haag, W. O.; Lago, R. M.; Weisz, P. B. *Faraday Discuss.* **1982**, *72*, 317−330.
(39) Santilli, D. S. *J. Catal.* **1986**, *99*, 327−334.
(40) Bleschmann, K.; Riekert, L. *J. Catal.* **1993**, *141*, 548−565.
(41) Arsenova-Hartel, N.; Bludau, H.; Schumacher, R.; Haag, W. O.; Karge, H. G.; Brunner, E.; Wild, U. *J. Catal.* **2000**, *191*, 326−331.
(42) Anderson, M. W.; Klinowski, J. *J. Am. Chem. Soc.* **1990**, *112*, 10−16.
(43) Santilli, D. S.; Harris, T. V.; Zones, S. I. *Microporous Mater.* **1993**, *1*, 329−341.

The trimethylbenzene selectivity of the chosen *m*-xylene disproportionation reaction is often assumed to be indicative of local pore shape. For example, a lower isomerization (xylene products) to disporportionation (trimethylbenzenes) ratio is assumed to imply that the reaction cavities are more spacious since they could better accommodate bulky transition states.

A compilation of experimental trimethylbenzene product selectives fails to show any clear evidence for transition state shape selectivity (Table 1). As has been noted previously, the selectivities are often within a few percentage points of the equilibrium values,[24] suggesting that the product distribution is not kinetically controlled. Fluctuations in the selectivities of around 2−3 percentage points appear to be attributable to variations in the sample and experimental conditions (see BEA, MOR, USY, and Y). In the situations where there is significant deviation from equilibrium, it is toward enrichment of the 1,2,4-trimethylbenzene isomer. A shift toward this fastest-diffusing isomer is fully explainable as a product shape selectivity effect. Unless one believes that the variations in the 1,2,3/1,3,5-trimethylbezene ratio are significant, *there is no evidence that the trimethylbenzene selectivity stems from transition state shape selectivity*.

What would be required to demonstrate transition state shape selectivity experimentally? There must be clear evidence that the *local* shape of the pore changes the *local* reaction rates to the product isomers. Changes in the local reaction rates imply that the rate determining transition states have changed if the reactant states are the same. If the reactants immediately before the limiting transition states are not identical, then it must also be shown that the rate changes are not due to varying stabilization of the reactants. Fulfillment of these criteria is very difficult because determination of the local reactant distribution, local reaction rates, and local product distribution for a series of pore types is a daunting task. Furthermore, product shape selectivity effects must be separated out or eliminated. If there is no potential for isomerization, no isomer-dependent diffusivities, no desorption activation energy differences, and no surface reactions, then the local reaction rates simplify to those measured externally. In practice, this means that product distributions inside the pores must be measured or independent diffusion studies of products must be made.

**1.2. Mechanistic Pathways.** The disproportionation of *m*-xylene results in one of the *m*-xylenes giving up a methyl group to become toluene. This methyl group adds to the other *m*-xylene, resulting in one of three possible trimethylbenzene products shown in Figure 1. It is in the local selectivity to these trimethylbenzene species that transition state shape selectivity is apparent. In this section, we examine the two most likely mechanistic pathways. A third pathway, involving the direct exchange of a methyl cation between rings, has been proposed,[46] but we consider it less likely because it is much more concerted and has higher (252−277 kJ/mol) activation energies than other steps (120−200 kJ/mol) as seen from cluster calculations.[46,47]

(44) Lourenco, J. P.; Ribeiro, M. F.; Ribeiro, F. R.; Rocha, J.; Gabelica, Z. *Appl. Catal., A* **1996**, *148*, 167−180.
(45) Wang, I.; Tsai, T. C.; Huang, S. T. *Ind. Eng. Chem. Res.* **1990**, *29*, 2005−2012.
(46) Blaszkowski, S. R.; Van Santen, R. A. In *Transition State Modeling for Catalysis*; Morokuma, K., Truhlar, D. G., Eds.; ACS Symposium Series 721; American Chemical Society: Washington, DC, 1999; pp 307−320.
(47) Rozanska, X.; Saintigny, X.; Santen, R. A. V.; Hutschka, F. *J. Catal.* **2001**, *202*, 141−155.

**Table 1.** Compilation of Trimethylbenzene Product Selectives from the *m*-Xylene Test Reaction Ordered by Selectivity to the 1,2,4-Trimethylbenzene Isomer[a]

| zeolite framework | percent selectivities | | | 1,2,3/1,3,5 | T (K), reference |
| --- | --- | --- | --- | --- | --- |
| | 1,2,3-TMB | 1,2,4-TMB | 1,3,5-TMB | | |
| OFF | NQ | 100 | NQ | | 590, [27] |
| NU-87 (NES) | 0 | 100 | 0 | | 590, [25] |
| SSZ-35 (STF) | 0 | 100 | 0 | | 590, [27] |
| SSZ-42 | NQ | 100 | NQ | | 590, [27] |
| SSZ-44 (SFF) | 0 | 100 | 0 | | 590, [27] |
| ZSM-5 (MFI) | 0 | 100 | 0 | | 590, 623, [27, 44] |
| ZSM-12 (MTW) | NQ | 100 | NQ | | 590, [27] |
| ZSM-48 | NQ | 100 | NQ | | 590, [27] |
| ZSM-50 (EUO) | NQ | 100 | NQ | | 590, [25] |
| IM-5 | 0.0 | 95.6 | 4.4 | 0.0 | 625, [29] |
| NU-87 (NES) | 4.6 | 94.0 | 1.4 | 3.3 | 625, [29] |
| CIT-5 (CFI) | 8 | 83.5 | 8.5 | 0.9 | 590, [27] |
| SSZ-24 | 9 | 83.5 | 7.5 | 1.2 | 590, [27] |
| (MOR) | 8.5 | 77.5 | 14 | 0.6 | 590, [27] |
| (MOR) | 8.1 | 70.9 | 21.0 | 0.4 | [44] |
| NU-86 | 6.7 | 75.2 | 18.1 | 0.4 | 625, [29] |
| SSZ-31 | 7 | 76 | 17 | 0.4 | 590, [27] |
| SSZ-33 | 8.5 | 72.5 | 19 | 0.4 | 590, [27] |
| CIT-1 (CON) | 10.0 | 72.0 | 18.0 | 0.6 | [25] |
| SSZ-26 | 8 | 71.5 | 20.5 | 0.4 | 590, [28] |
| UTD-1 (DON) | 7 | 71 | 22 | 0.3 | 590, [27] |
| Beta (BEA) | 8 | 67 | 25 | 0.3 | 590, [27] |
| Beta (BEA) | 7 | 67 | 26 | 0.3 | 623, [23] |
| Beta (BEA) | 9 | 62 | 29 | 0.3 | 618, [45] |
| SAPO-37 | NQ | 67.0 | 33.0 | | [44] |
| SAPO-40 (AFR) | 7.8 | 66.3 | 25.9 | 0.3 | [44] |
| USY (FAU) | 6.5 | 66 | 27.5 | 0.2 | 590, [27] |
| USY (FAU) | 9.4 | 65.3 | 25.3 | 0.4 | 621, [45] |
| USY (FAU) | 8.0 | 63.6 | 28.4 | 0.3 | [44] |
| Y (FAU) | 9.8 | 65.4 | 25.8 | 0.4 | 621, [45] |
| Y (FAU) | 7.7 | 64.6 | 27.7 | 0.3 | [44] |
| L (LTL) | 7.0 | 63.5 | 29.5 | 0.2 | 590, [27] |
| **equilibrium, 623 K** | **8** | **68** | **24** | **0.3** | [22, 44] |

[a] In most cases, the selectives are quite similar to the equilibrium selectivity. If there is a significant deviation from equilibrium, then it is toward enrichment of the 1,2,4-trimethylbenzene isomer. Enhanced production of the fastest diffusing 1,2,4-trimethylbenzene isomer would be expected if product shape selectivity was operative. Experimental conversions, when specified, were between 5 and 20%. NQ = not quantifiable.

The critical points on the potential energy surfaces of these two pathways will form the basis for discussion of shape selectivity in the next section.
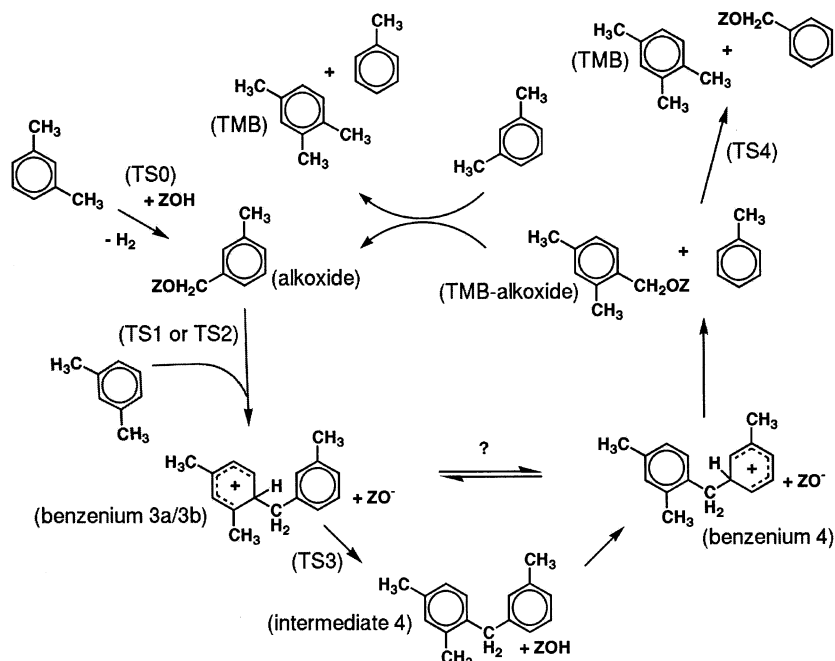
The two pathways differ predominantly in the activated form of the transferring methyl group. In the diphenylmethane-mediated pathway, the zeolite extracts a hydride from *m*-xylene to form a carbenium ion at one of the methyl groups (the alkoxide is shown in Figure 2). This carbenium ion then adds to a second *m*-xylene to form a methyl-substituted diphenylmethane species 3a/3b with an extra proton at one of the methyl ring positions. Migration of the proton to the other ring and subsequent dissociation of the two rings lead to a toluene and a zeolite-associated trimethylbenzene cation. To continue the catalytic cycle, the trimethylbenzene species abstracts a hydride group from another methyl-substituted aromatic. In contrast, the activated form in the methoxide-mediated pathway is a $CH_3^+$ group bound to a zeolitic oxygen (a methoxide species). The zeolite exchanges its acidic proton for the methyl group in the two-step process shown in Figure 3. This methoxide group is then free to add to the ring of another *m*-xylene molecule. The resulting trimethylbenzene donates its extra proton back to the zeolite to complete the catalytic cycle in Figure 4.

**Figure 2.** Schematic of the diphenylmethane-mediated reaction pathway. The cycle is initiated when the acidic proton abstracts a hydride from a methyl group of a *m*-xylene molecule. Once this step occurs and fresh *m*-xylene is available, the cycle can be repeated indefinitely to result in the net transfer of a methyl group from one *m*-xylene to another.
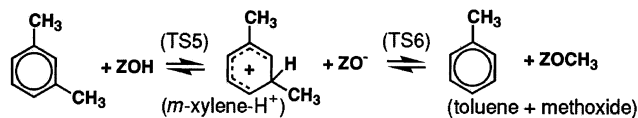


**Figure 3.** Schematic of the methoxide-formation reaction pathway. The active methoxide ($ZO-CH_3$) is formed by exchanging a zeolite proton for a methyl group from *m*-xylene.
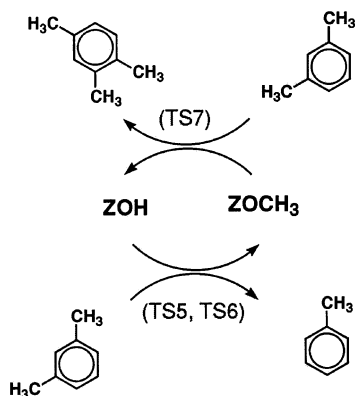


**Figure 4.** Schematic of the methoxide-mediated disporportionation cycle. A methyl group is transferred from one *m*-xylene to another via a regenerable methoxide ($ZO-CH_3$) intermediate.

The size of the transition state structures and the intermediates will be critical in producing selectivity effects due to the shape of the local environment. The diphenylmethane-mediated pathway passes through bulky biphenyl species that may be too large to form in some zeolite pores. Despite the bulkiness, existence of this pathway is assumed in the literature.[48] Early speculation based on ratios of toluene to ethylbenzene transalkylation suggested that the pathway was absent in the relatively restricted pores of HZSM-5.[39] More recent isotope-labeling experiments

during toluene disproportionation show that fully deuterating the toluene methyl group results in a distribution of deuterated species.[49] No such scrambling is expected from the methoxide-mediated mechanism, so either the diphenylmethane-mediated mechanism is at least partially operative or another pathway is scrambling the methyl deuteriums. Scrambling from H/D exchange is a strong possibility since the activation energy barriers for benzene (80−90 kJ/mol[50]) are equivalent or lower than the barriers to be calculated here. Isotope labeling has also been conducted to study isomerization mechanisms.[51] Reaction of undeuterated *p*-xylene with fully deuterated methyl groups results in xylenes with mixed methyl groups. The authors take this as support for a bulkier bimolecular pathway, though the possibility of a methoxide-mediated mechanism is not excluded. The effect is more prevalent over an HY (FAU framework) catalyst than in the BEA framework, implying that tighter pores do tend to favor pathways that avoid bulky intermediates or transition states.

There is no direct evidence showing that the methoxide-mediated disproportionation pathway occurs. However, strong support comes from the study of the methoxide species and of other aromatic reactions in zeolites. Methoxide species have been observed using both MAS NMR[52,53] and IR[54] techniques. The existence of the same species is supported by quantum chemical methods,[55,56] and a semiempirical study found that reaction with toluene is reasonable.[57] The clearest evidence

(48) Olah, G. A.; Molnar, A. *Hydrocarbon Chemistry*; Wiley: New York, NY, 1995.

(49) Xiong, Y. S.; Rodewald, P. G.; Chang, C. D. *J. Am. Chem. Soc.* **1995**, *117*, 9427−9431.
(50) Beck, L. W.; Xu, T.; Nicholas, J. B.; Haw, J. F. *J. Am. Chem. Soc.* **1995**, *117*, 11594−11595.
(51) Corma, A.; Sastre, E. *J. Catal.* **1991**, *129*, 177−185.
(52) Murray, D. K.; Chang, J. W.; Haw, J. F. *J. Am. Chem. Soc.* **1993**, *115*, 4732−4741.
(53) Seiler, M.; Schenk, U.; Hunger, M. *Catal. Lett.* **1999**, *62*, 2−4.
(54) Mirth, G.; Lercher, J. A. *J. Phys. Chem.* **1991**, *95*, 3736−3740.
(55) Zicovich-Wilson, C. M.; Viruela, P.; Corma, A. *J. Phys. Chem.* **1995**, *99*, 13224−13231.
(56) Blaszkowski, S. R.; Van Santen, R. A. *J. Phys. Chem.* **1995**, *99*, 11728−11738.

comes from Ivanova and Corma's observed depletion of MAS NMR lines assigned to methoxide during formation of xylenes.[58]

Corma et al. derived intrinsic activation barriers for *m*-xylene transalkylation of 85 to 119 kJ/mol from kinetic data for a variety of zeolite HY catalysts.[59] No clear dependence on aluminum content was observed. However, the steam dealuminated catalysts generally had lower activation energies. The opening of the framework during the steaming procedure may be important in reducing diffusion limitations and thereby lowering the observed activation energy. The test reaction conditions are approximately 600 K, atmospheric pressure, and with conversions in the 5% to 15% range.[23−29]

**1.3. Theoretical Work to Date.** Force-field-based molecular mechanics methods can be used to probe diffusivities and the fit between the molecular and pore geometry of molecules confined in zeolite pores. Santilli et al. were first to relate the simulated fit of molecules to a concept of shape selectivity.[43] Macedonia and Maginn used biased Monte Carlo integration of transition state analogues to gather mechanistic information on a classic transition state shape selective reaction.[60] Schenk et al.'s use of a similar biased Monte Carlo technique helped them relate the fit of possible branched hydrocarbon reaction products to reaction pathways.[61] Anderson et al. followed by using similar studies of reactants and transition state analogues to attempt selectivity predictions.[62] Turner et al. extended an older grand canonical ensemble method for studying equilibrium reactant and product distributions in confined spaces to reaction rate prediction using transition state energy and structure information.[63] The type of information gathered from these force field simulations could also be used in a lattice-based simulation to study combined diffusion and reaction, such as seen in product shape selectivity.[64,65]

The use of electronic structure techniques to treat bond-breaking and bond-forming processes is necessary for an accurate description of transition state shape selectivity. It obviates the need to assume the characteristics of a transition state analogue. Šponer et al. used simple geometry constraints during standard quantum chemistry calculations to mimic environment shape.[66] More recently they used an unspecified method to investigate the fit and therefore reactivity of geometry optimized xylene structures in various pore types.[67] Song et al. used semiempirical calculations to identify site reactivity tendencies and related these to the shape of the product, but these should not be considered a shape selectivity effect because pore shape was not a factor. Clark et al. developed a novel method using the overlap of precalculated molecular Fukui functions to study steric reactivity effects for an ensemble.[68]

The method was able to examine transition state shape selectivity[18] but is restricted by various assumptions.

Only very recently has it become possible to treat a system large enough to explicitly include environmental effects on hydrocarbon reactions using electronic structure methods.[16,20] Density functional theory (DFT) calculations which applied periodic boundary conditions predicted significant steric effects for the alkylation of toluene with methanol in H-MOR[16] and demonstrated activation energy variations across different frameworks for the chemisorption of isobutene.[20] However, these calculations are still so demanding that second energy derivatives needed to characterize stationary points and to estimate entropy effects were not calculated for the periodic models.

## 2. Computational Methodology

We have developed a mixed quantum mechanical−molecular mechanical (QM/MM) method for examining zeolite reactions that avoids the limitations of pure DFT calculations.[19] It is ideally suited for examining local shape selectivity effects because it focuses the computational effort where it is most needed. The hydrocarbon molecules and a small $((OH)_2Al(OSi(OH)_3)_2)$ active portion of the zeolite are handled using a reliable DFT method, the B3LYP functional,[69−71] and a DZP/TZP basis set.[72] The less demanding remainder of the zeolite is treated with a flexible, polarizable, DFT-parametrized shell model that reproduces experimental infrared spectra.[73] The interactions between the hydrocarbon and the zeolite are described by a combination of Lennard−Jones terms from the literature and point charges from fits to the QM electrostatic potential (see Supporting Information section). The Lennard−Jones parameters are from previous work[74] and have been shown to reproduce hydrocarbon adsorption well with similar parameters.

This QM/MM hybrid approach has two advantages compared to full DFT calculations. It reduces the computational effort significantly enabling us to treat much larger systems, and it produces more reliable adsorption energies as shown before.[76] The favorable scaling of the QM/MM combination also makes possible full analytic evaluation of second energy derivatives and thereby both complete classification of the stationary points and estimates of free energy effects within the harmonic approximation.

The reliability of the methodology was established in previous work[19,76,77] and will be reviewed briefly. The most stringent test of a QM/MM approach is convergence of the results toward the full QM limit with increasing cluster size. Such tests have been made for the deprotonation energies of zeolites and for the energy barriers for proton jumps between different oxygen sites of the framework. For the O1 and O4 positions of FAU, the deprotonation energies change from 1155 to 1151 kJ/mol and from 1133 to 1137 kJ/mol, respectively, when the larger QM cluster models of ref 73 including 8 T atoms instead of 3 are used. Adding an additional shell of Si and O atoms (shell-5 model) causes a reduction by just 2 kJ/mol.[78] The energy barrier for the proton

(57) Corma, A.; Sastre, G.; Viruela, P. M. *J. Mol. Catal. A* **1995**, *100*, 75−85.
(58) Ivanova, I. I.; Corma, A. *J. Phys. Chem. B* **1997**, *101*, 547−551.
(59) Corma, A.; Llopis, F.; Monton, J. B. *J. Catal.* **1993**, *140*, 384−394.
(60) Macedonia, M. D.; Maginn, E. J. *AIChE J.* **2000**, *46*, 2504−2517.
(61) Schenk, M.; Smit, B.; Vlugt, T. J. H.; Maesen, T. L. M. *Angew. Chem., Int. Ed.* **2001**, *40*, 736−739.
(62) Anderson, B. G.; Schumacher, R. R.; Duren, R. V.; Singh, A. P.; Santen, R. A. V. *J. Mol. Catal. A* **2002**, *181*, 291−301.
(63) Turner, C. H.; Brennan, J. K.; Johnson, J. K.; Gubbins, K. E. *J. Chem. Phys.* **2002**, *116*, 2138−2148.
(64) Klemm, E.; Wang, J.; Emig, G. *Chem. Eng. Sci.* **1997**, *52* (18), 3173−3182.
(65) Klemm, E.; Scheidat, H.; Emig, G. *Chem. Eng. Sci.* **1997**, *52* (16), 2757−2768.
(66) Šponer, J.; Čejka, J.; Wichterlová, B. *J. Phys. Chem. B* **1998**, *102*, 7169−7175.
(67) Šponer, J. E.; Šponer, J.; Čejka, J. *THEOCHEM* **2001**, *540*, 145−152.
(68) Clark, L. A.; Ellis, D. E.; Snurr, R. Q. *J. Chem. Phys.* **2001**, *114*, 2580−2591.

(69) Becke, A. D. *Phys. Rev. A* **1988**, *38*, 3908−3100.
(70) Lee, C.; Yang, W.; Parr, R. G. *Phys. Rev. B* **1988**, *37*, 785−789.
(71) Becke, A. D. *J. Chem. Phys.* **1993**, *98*, 5648−5652.
(72) Schäfer, A.; Horn, H.; Ahlrichs, R. *J. Chem. Phys.* **1992**, *97*, 2571−2577.
(73) Sierka, M.; Sauer, J. *Faraday Discuss.* **1997**, *106*, 41−62.
(74) Lennard−Jones interactions are defined between the hydrocarbon atoms and the zeolite oxygens. The parameters were taken from previous work and have been shown to reproduce adsorption well with similar charges.[75] These parameters are: $\sigma_{H-O} = 2.6059$ Å, $\epsilon_{H-O} = 49.0901$ K, $\sigma_{C-O} = 3.0068$ Å, $\epsilon_{C-O} = 73.5985$ K.
(75) Snurr, R. Q.; Bell, A. T.; Theodorou, D. N. *J. Phys. Chem.* **1993**, *97*, 13742−13752.
(76) Clark, L. A.; Sierka, M.; Sauer, J. *J. Am. Chem. Soc.* **2003**, *125*, 2136−2141.
(77) Sierka, M.; Sauer, J. *J. Phys. Chem. B* **2001**, *105*, 1603−1613.
(78) Eichler, U.; Brändle, M.; Sauer, J. *J. Phys. Chem. B* **1997**, *101*, 10035−10050.

jump between the O1 and O4 positions changes from 107 kJ/mol for the present 3 T model[79] to 101 kJ/mol for an 8 T model and 95 kJ/mol for a large 23 T model.[77] For zeolite CHA, comparison is possible with full periodic QM calculations with the same functional (B3LYP).[19] For six proton jump barriers between 71 and 105 kJ/mol, the error of the 3 T embedded cluster result compared to the full periodic limit is between 6 and 0 kJ/mol.

Full periodic DFT calculations on systems of interest for the present study have also been made, and details are given in ref 76. Since plane wave basis sets are not efficient with hybrid functionals, the PBE functional is employed instead of B3LYP and exactly the same results cannot be expected. For the deprotonation energy of CHA, full periodic PBE calculations yield 1192 kJ/mol,[80] while embedded B3LYP calculations (QM/MM) yield 1181 kJ/mol.[81] For a proton-transfer reaction between the benzenium-type intermediate 3b and the deprotonated zeolite FAU yielding intermediate 4 (TS3, see Figure 9), the periodic PBE calculations predict a barrier of 66 kJ/mol, while embedded B3LYP calculations (QM/MM) yield 47 kJ/mol.[76] For the energy difference between the alkoxide O(4) (Figures 2 and 9) and the carbenium ion formed by dissociation of the C−O bond between the hydrocarbon and the zeolite framework, periodic PBE yields again a larger value than embedded B3LYP (QM/MM), 63 compared to 53 kJ/mol.[76] We conclude that full periodic DFT calculations and the present QM/MM hybrid calculations yield very similar results and that observed differences are largely due to different functionals.

For hydrocarbon reactions in zeolites, there is an important limitation of DFT. While current density functionals are well suited for describing bond breaking−bond making steps, they fail to yield reliable energies for van der Waals (dispersion) interactions (see ref 82 and references therein) which dominate the adsorption−desorption steps. In our previous study,[76] we showed that full periodic DFT calculations predict an adsorption energy of 28 kJ/mol for *m*-xylene in H-FAU. An estimate for the electronic energy of adsorption derived from available experimental heats of adsorption and from calculated zero point vibrational energies is 67 to 73 kJ/mol. Force field calculations are known to provide a good description of van der Waals interactions in general and of zeolite adsorption energies in particular. Our QM/MM hybrid approach takes advantage of this by limiting the DFT description to a small model of the active site and the hydrocarbon molecule, while all the other interactions including the interactions between the hydrocarbon and the zeolite wall are described by the force field. Indeed, the QM/MM result for the *m*-xylene adsorption energy is 61 kJ/mol very close to the experimental estimate.

Hence, when a comparison is made between our QM/MM embedding results and the computationally more demanding full DFT plane wave calculations, within limitations due to different functionals/basis sets, we expect the two methods to yield similar results for hydrocarbon reactions inside zeolite channels where changes in van der Waals energies are minor. For other reactions, particularly those involving adsorption or desorption, our QM/MM embedding technique is expected to be an improvement because van der Waals interactions are included in the MM part.

Despite the demonstrated success of the computational methodology, it is important to understand its potential limitations. The mechanical embedding method used here does not explicitly account for electronic polarization of the QM portion by the MM environment. The QM part is not polarized by surrounding charges, but mutual polarization of the

framework and the active site is included at the shell model force field level.

Another source of some uncertainty is the choice of atomic point charges employed in the MM force field representation. The charges on the hydrocarbon are chosen such that they reproduce the electrostatic potential obtained by DFT calculations for the QM model (potential derived charges).[76] However, the fit is not unique, and for the alkoxide structures there is variability in charge partitioning between the zeolite model and the hydrocarbon part (which is described by fractional charges). Moreover, we combine the shell model charges on the zeolite part, as dictated by the proven zeolite force field, with fractional charges on the hydrocarbon part. Despite uncertainties in the choice of charges, the polarizability of the shell model avoids potential problems with immobile charges.[83]

A study of only the transition state structure, as performed here, rather than the entire dividing surface, could insufficiently characterize the local environment effects on the barrier to reaction. In a system characterized by reactant and product potential energy basins with $N$ degrees of freedom, the dividing surface is the $N$-1-dimensional surface of zero-gradient points separating the two basins and passing through the transition state.[84−86] In this work, we use the harmonic approximation and classical transition state theory to obtain entropic information about the dividing surface near the transition state. Since reactions do not exclusively proceed through the first-order transition state (see ref 87 for an example), any variation in the environment shape effects across the full dividing surface will not be captured by looking only at the transition state structure and the local dividing surface through the harmonic approximation. Some of the Monte Carlo methods above account for this variability by making strong assumptions about the transition state ensemble and using parametrized potential functions for evaluating the potential energy.[60,62,63,68] Here we avoid these assumptions but provide rigorous characterization of only the transition state structure. In doing so, we minimize the error for the dominating energy barrier and still get an estimate of the importance of free energy corrections to these barriers.

Zeolite simulation cells were constructed from the published crystallographic data for FAU,[88] MOR,[89] and MFI.[90] Constant pressure optimizations without the hydrocarbons using the shell model[73] and the GULP code[91] were used to determine the unit cell geometry. Constant volume optimizations then determined starting conditions for the QM/MM simulations. A double unit cell in the *z*-direction is used for MOR to ensure sufficient separation between images. The cell parameters are (Å, degree): FAU $a = 17.4298$, $b = 17.4925$, $c = 17.4856$, $\alpha = 59.8709$, $\beta = 59.8981$, $\gamma = 59.9960$; MFI $a = 20.3920$, $b = 19.8097$, $c = 13.5360$, $\alpha = \beta = \gamma = 90.0$; MOR $a = 18.2006$, $b = 20.6271$, $c = 15.2146$, $\alpha = \beta = \gamma = 90.0$.

Proton positions were chosen based on indications of site stability and accessibility to the relatively bulky hydrocarbons. For the FAU framework, the two lowest energy positions of four possibilities are chosen.[76] Brändle and Sauer examined the same frameworks with a similar shell model and QM/MM calculations.[92] In the MOR framework, the Al4−O2(H)−Si site near the entrance to the side pocket is chosen for its marginal stability from a pool of 14 possibilities. The Al12−O24(H)−Si12 site in the MFI framework is chosen from 96 possibilities

(79) Sauer, J.; Sierka, M.; Haase, F. In *Transition State Modeling for Catalysis*; Morokuma, K., Truhlar, D. G., Eds.; ACS Symposium Series 721; American Chemical Society: Washington, DC, 1999; pp 358−367.

(80) Tuma, C. Zum Einsatz ebener Wellen und atomarer Pseudopotentiale in Dichtefunktionalrechnungen und Kombination mit störungstheoretischen Methoden. Diplom Thesis, Humboldt-Universität, Berlin, 2000.

(81) Sauer, J.; Schröder, K. P.; Termath, V. *Collect. Czech. Chem. Commun.* **1998**, *63*, 1394−1408.

(82) Wesolowski, T. A.; Parisel, O.; Ellinger, Y.; Weber, J. *J. Phys. Chem. A* **1997**, *101*, 7818−7825.

(83) Clark, L. A.; Snurr, R. Q. *Chem. Phys. Lett.* **1999**, *308*, 155−159.

(84) Heidrich, D.; Kliesch, W.; Quapp, W. *Properties of Chemically Interesting Potential Energy Surfaces*; Lecture Notes in Chemistry. Spring-Verlag: Berlin, 1991.

(85) Sevick, E. M.; Bell, A. T.; Theodorou, D. N. *J. Chem. Phys.* **1993**, *98*, 3196−3212.

(86) Ruedenberg, K.; Sun, J. Q. *J. Chem. Phys.* **1994**, *100*, 5836−5848.

(87) Ammal, S. C.; Yamataka, H.; Aida, M.; Dupuis, M. *Science* **2003**, *299*, 1555−1557.
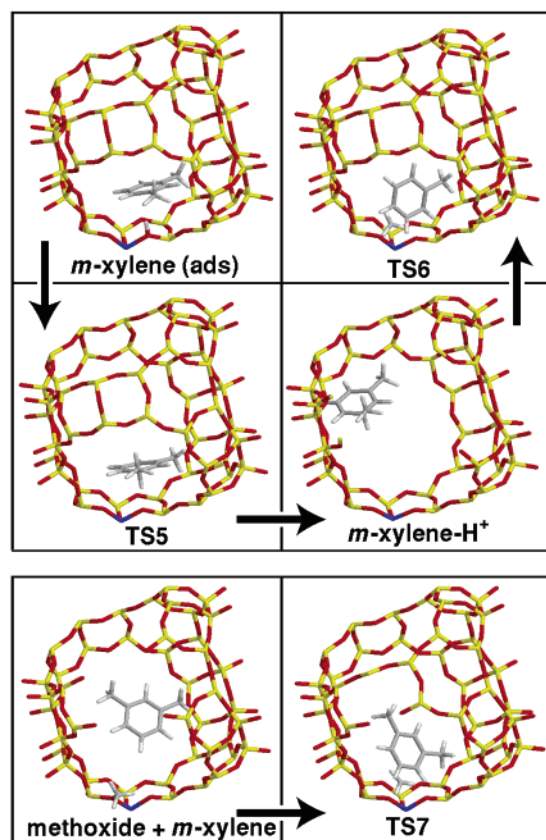
(88) Olson, D. H. *J. Phys. Chem.* **1970**, *74*, 2758−2764.

(89) Alberti, A.; Davoli, P.; Vezzalini, G. *Z. Kristallogr.* **1986**, *175*, 249−256.

(90) van Koningsveld, H.; van Bekkum, H.; Jansen, J. C. *Acta Crystallogr.* **1987**, *B43*, 127−132.

(91) Gale, J. D. *J. Chem. Soc., Faraday Trans.* **1997**, *93*, 629−637.

(92) Brändle, M.; Sauer, J. *J. Am. Chem. Soc.* **1998**, *120*, 1556−1570.
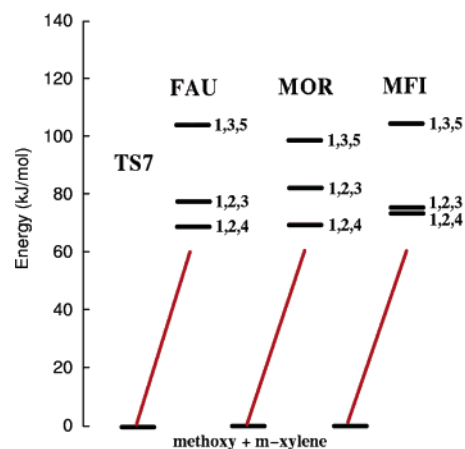
**Figure 5.** Structures for the methoxide-mediated disproportionation reaction. Top: formation of the methoxide species by exchange of zeolite proton for methyl group. Bottom: Shape selective formation of the TMB alkoxide. Portions of the zeolite have been removed to clarify the position of the molecules.

due to its comparatively low energy and position in the intersections where it is most accessible to the aromatic reactants.

## 3. Results and Discussion

We examine first the methoxide-mediated pathway in the FAU framework up to the transition state where the selectivity-determining carbon−carbon bond is formed. This same transition state will then be compared to its analogues in the MFI and MOR frameworks to directly address the effect of environmental shape. In the following section, comparison is made to the more complex diphenylmethane-mediated mechanism in only the FAU framework, showing that there is no clear and overwhelming pathway preference. Consequently, the transition state shape selectivity seen in the methoxide-mediated pathway can be expected to be important in determining observable effects. Furthermore, in the more restricted MFI and MOR frameworks, the less bulky methoxide-mediated mechanism can be expected to be increasingly dominant.

**3.1. Methoxide-Mediated Pathway.** The important structures in the methoxide formation reaction (see Figure 3) in the FAU framework are shown in Figure 5 (top panel). Addition of the zeolite proton to the ring during TS5 results in an activated species that may then give up its methyl group at the same ring position during TS6. Loss of the methyl group (TS6) is rate-determining with a ZPE-corrected potential energy barrier of 136 kJ/mol. The free energy corrections given in Table 2 do not change the relative importance of the proton addition versus the methyl group loss steps.

**Figure 6.** Comparison of the transition state structure potential energies (QM/MM) for the methoxide-mediated shape selectivity step in the three framework types. The energetic ordering of the transition state structures for the three isomers is unchanged across the frameworks. All transition state structures energies are shown relative to the methoxide + *m*-xylene state in the same framework.

The final back-donation of the extra proton on the TMB-H$^+$ molecule (after TS7) to form the product isomer is unlikely to have a higher barrier than methylation. Comparison of the proton-transfer (TS5) and the methylation (TS6) steps, which have one fewer methyl group, shows that the methylation barrier (*m*-xylene-H$^+$ → TS6) is clearly higher than the back-protonation (*m*-xylene-H$^+$ → TS5) barrier. The lower barrier means that it will not control the selectivity of the overall methoxide-mediated pathway.

A fewer number of atoms and the comparatively bound nature of the selectivity-determining step in the methoxide-mediated pathway make it a computational tractable candidate for comparison across framework geometries. The structures in the FAU framework that compose this critical methyl transfer step are shown in Figure 5. In addition to the FAU framework, a single likely acid site location is chosen for each of the MFI and MOR zeolites and the methoxide group addition barrier to a *m*-xylene molecule is determined. Figure 6, in conjunction with the numerical details in Tables 2 and 3, shows that *the qualitative ordering of the potential energy barriers to the three isomers is unchanged by the framework geometry*. In each case, the selectivity preference is 1,2,4 > 1,2,3 > 1,3,5. The ZPE-corrected energy barriers for the 1,2,3 isomer are 1−16 kJ/mol higher than those for the 1,2,4 isomer, and for the 1,3,5 isomers, they are 30−34 kJ/mol higher than those for the 1,2,4 isomer.

Corrections for vibrational free energy effects make the favored selectivity to the 1,2,4 isomer less clear. While the selectivity to the 1,2,4 isomer is maintained in MOR, in FAU the free energy barrier to the 1,2,4 isomer is only insignificantly lower (1 kJ/mol) than to the 1,2,3 isomer. In the MFI framework, the free energy contribution is sufficient to shift the selectivity to the 1,2,3 isomer. Despite the vibrational free energy corrections, the barriers to the 1,3,5 isomer remain the highest across the isomers.

The geometric differences in the transition states across framework types can be large before they affect the relative energies. Figure 7 shows all nine transition state structures for the critical methoxide addition step arranged so that the *m*-xylene molecule is always in the same orientation. There is little critical carbon−carbon or carbon−oxygen bond length variation (ca.

**Table 2.** Relative Potential Energies for the Methoxide-Mediated Intermediates and Transition State Structures in the FAU, MOR, and MFI Frameworks as Shown in Figure 5[a]

| state | system energies in kJ/mol | | | | | $\ln(q/q^*)$[c] | freq (cm$^{-1}$) |
|---|---|---|---|---|---|---|---|
| | QM/MM + ZPE | A[b]-ZPE | QM/MM | QM | MM | | |
| | Methoxide Formation in FAU | | | | | | |
| *m*-xylene (ads.) | 0 | 0 | 0 | 0 | 0 | 0.00 | |
| TS5 | 112 | 18 | 118 | −55 | 172 | −3.42 | 120*i* |
| *m*-xylene-H$^+$ | 4 | 8 | 5 | −372 | 377 | −1.54 | |
| TS6 | 141 | 7 | 145 | −92 | 237 | −1.36 | 251*i* |
| FAU | | | | | | | |
| methoxide + *m*-xylene (ads.) | 0 | 0 | 0 | 0 | 0 | 0.00 | |
| TS7, 1,2,3-TMB-H$^+$ | 71 | 19 | 78 | −69 | 147 | −3.70 | 337*i* |
| TS7, 1,2,4-TMB-H$^+$ | 63 | 26 | 69 | −71 | 141 | −5.08 | 332*i* |
| TS7, 1,3,5-TMB-H$^+$ | 97 | 14 | 105 | −46 | 151 | −2.73 | 239*i* |
| MOR | | | | | | | |
| methoxide + *m*-xylene (ads.) | 0 | 0 | 0 | 0 | 0 | 0.00 | |
| TS7, 1,2,3-TMB-H$^+$ | 79 | 25 | 82 | −82 | 164 | −4.73 | 390*i* |
| TS7, 1,2,4-TMB-H$^+$ | 63 | 16 | 69 | −100 | 169 | −3.05 | 369*i* |
| TS7, 1,3,5-TMB-H$^+$ | 94 | 26 | 99 | −76 | 175 | −5.11 | 301*i* |
| MFI | | | | | | | |
| methoxide + *m*-xylene (ads.) | 0 | 0 | 0 | 0 | 0 | 0.00 | |
| TS7, 1,2,3-TMB-H$^+$ | 71 | 2 | 75 | −67 | 141 | −0.47 | 347*i* |
| TS7, 1,2,4-TMB-H$^+$ | 70 | 13 | 73 | −90 | 163 | −2.53 | 340*i* |
| TS7, 1,3,5-TMB-H$^+$ | 99 | −3 | 105 | −57 | 162 | 0.64 | 291*i* |

[a] Potential energies are broken into QM and MM contributions and have separate zeros for each section of the table. See Table 3 for reference energies. Temperature-dependent entropic effects are calculated from the harmonic approximation at 623 K. Reference system energies are given in Table 3. [b] Vibrational Helmholtz free energies (*A*) are calculated from the harmonic partition function and include the ZPE contribution. [c] The ratio of state (*q*) to reference state (*q**) partition functions does not include the ZPE contribution.

**Table 3.** Energies for Reference Structures

| state | reference system energies in kJ/mol | | | | |
|---|---|---|---|---|---|
| | QM/MM | QM | MM | A[a] | ZPE |
| *m*-xylene (ads. in FAU) | −5 507 442.2 | −4 962 397.9 | −545 044.3 | 501.9 | 1907.1 |
| alkoxide O(1) + *m*-xylene (ads.) | −6 320 022.6 | −5 774 826.2 | −545 196.4 | 776.0 | 2270.2 |
| methoxide + *m*-xylene (ads.) | | | | | |
| structures: | | | | | |
| FAU | −5 610 533.7 | −5 065 457.5 | −545 076.2 | 541.9 | 1982.7 |
| MOR | −6 210 293.4 | −5 065 451.0 | −1 144 842.4 | 619.3 | 3438.2 |
| MFI | −6 210 509.0 | −5 065 440.2 | −1 145 068.8 | 522.3 | 3409.9 |

[a] See footnote *b* of Table 2.

0.05 Å) and no apparent correlation to activation energy. In contrast, the angle of approach and the shape of the active site, as represented by the QM cluster, may vary greatly. The closest oxygen atom to the central methoxide carbon also varies across the structures. It appears that there is enough geometric approach flexibility to allow the transition state structures to find similar relative energies across the frameworks.

There are small but consistent differences in the imaginary frequencies across the frameworks. In particular, the consistency of the ordering of frequencies for each isomer across frameworks (1,3,5 ≪ 1,2,4 < 1,2,3) suggests that a correlation exists. The most open framework, FAU, has the lowest magnitude frequencies and therefore the least curvature along the reaction mode. One would expect greater spatial constraints to curve the surface more at the transition state, and indeed, frequencies in the more-confined MFI and MOR pores are higher. However, while there is no clearly definable difference in size between the intersection site in MFI and the main pore site in MOR, the energy profiles along the reaction modes are consistently more curved in MOR. The free energy corrections in MOR are noticeably more positive than those in other frameworks, lending support to the idea that constrictions are greater. Since it is not size, it could be a shape variation that is responsible for the reaction mode frequencies differences in MOR.

Comparison to previous computational results allows estimation of methodology, degree of aromatic substitution, and water effects. Blaszkowski et al.[46] studied addition of methoxide to toluene over a small (HOHAl(OH)$_3$) cluster using a DFT functional (Becke−Perdew) without exact exchange contributions. They found small (ca. 7 kJ/mol) differences between activation energies to the three xylene isomers and no preference between the favored para and ortho isomers. Their activation energies (183−190 kJ/mol) were significantly higher than ours (69−105 kJ/mol for TS7 step), presumably due to overestimation of the barriers in the cluster-only calculations and stabilization of the TS in our more methylated aromatic ring. Their work also suggests that the presence of water decreases the activation barrier by 59−62 kJ/mol,[46] with little dependence on product isomer.

Another example of such overestimation from cluster calculation can be seen in the protonation of the aromatic ring at the methyl position. Rozanska et al.[47] used a (Al(OHSiH$_3$)-(OSiH$_3$)$_2$(OH)) cluster and the same B3LYP functional that we employ to calculate an activation energy of 201 kJ/mol for toluene protonation. The difference of 87 kJ/mol compared to our 114 kJ/mol for *m*-xylene protonation (TS5) is too large to be attributed solely to methyl substitution effects.[93] A similar difference of 68 kJ/mol (209 kJ/mol[47] vs 141 kJ/mol at TS6) is
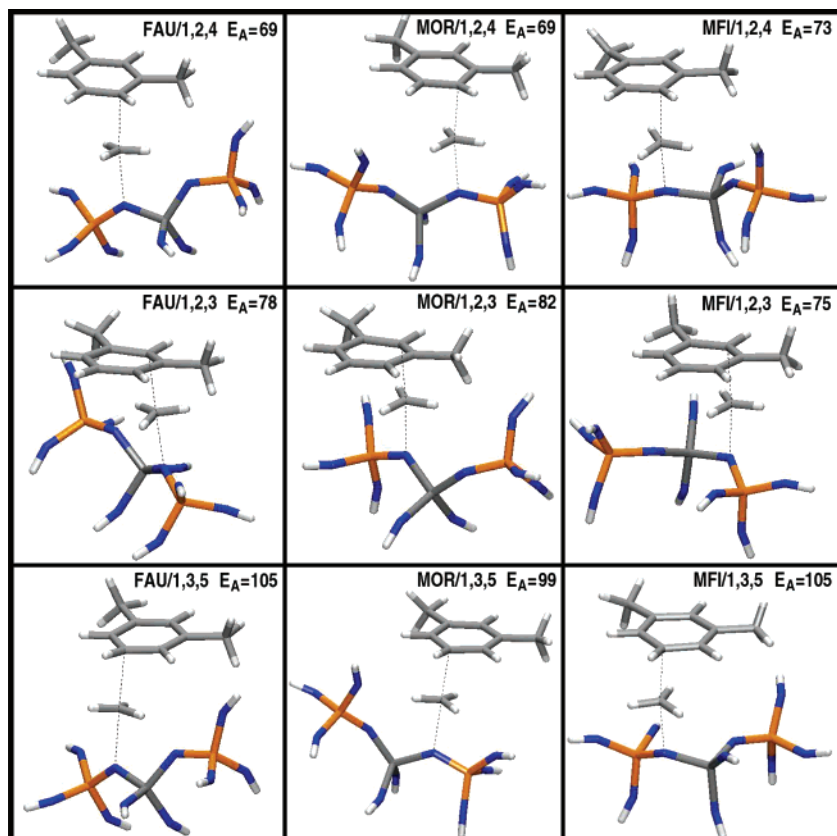
**Figure 7.** Comparison of the methoxide-mediated transition state structures across variations in zeolite and product trimethylbenzene isomer. There is little variation in the critical bond lengths but a great deal of variation in the orientations with respect to the zeolite. Despite structure differences, there is little variation in the activation energies across the zeolites. Only the QM portion of the system is shown for clarity. Activation energies ($E_A$) are given in kJ/mol.

seen at the methoxide formation step. For this step, Blaskowski et al. calculate an even larger barrier of 240 kJ/mol.[46] Cluster calculations appear to give barriers that are too high by at least 50 kJ/mol.

The spread of activation energy barriers to product isomers provides a way to quantify bulkiness contributions to transition state shape selectivity. Comparable periodic calculations using full DFT (Perdew−Wang91 functional) results are available for methoxide addition to toluene in the MOR framework. Rozanska et al.[17] see a difference of 15 kJ/mol between the highest and lowest activation energies. This is larger than the 7 kJ/mol seen by Blaszkowski et al.,[46] presumably because environment effects are included. The magnitude of their activation energies (86 to 101 kJ/mol) is similar to ours in MOR (69 to 99 kJ/mol). However, our highest-to-lowest difference is larger (30 kJ/mol), suggesting that the comparative bulkiness of the *m*-xylene contributes to greater selectivity differences.

**3.2. Diphenylmethane-Mediated Pathway.** Due to the complexity of the disproportionation reaction pathway, we examine it only in the FAU framework. The intention is to show that the rate-determining activation barriers are similar to those in the methoxide-mediated pathway. The more complex pathway also provides examples of how a reaction step that does not directly produce selectivity-defining bonds can nevertheless change the selectivity.

Reaction pathway structures are shown in Figure 8, the corresponding potential energy surface schematic is shown in

(93) Arstad, B.; Kolboe, S.; Swang, O. *J. Phys. Chem. B* **2002**, *106*, 12722−12726.
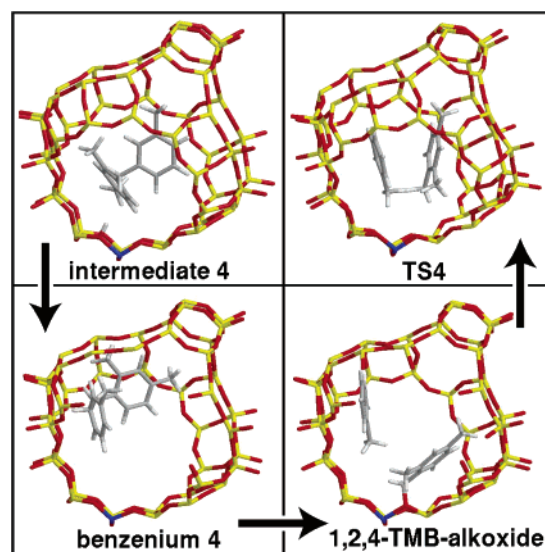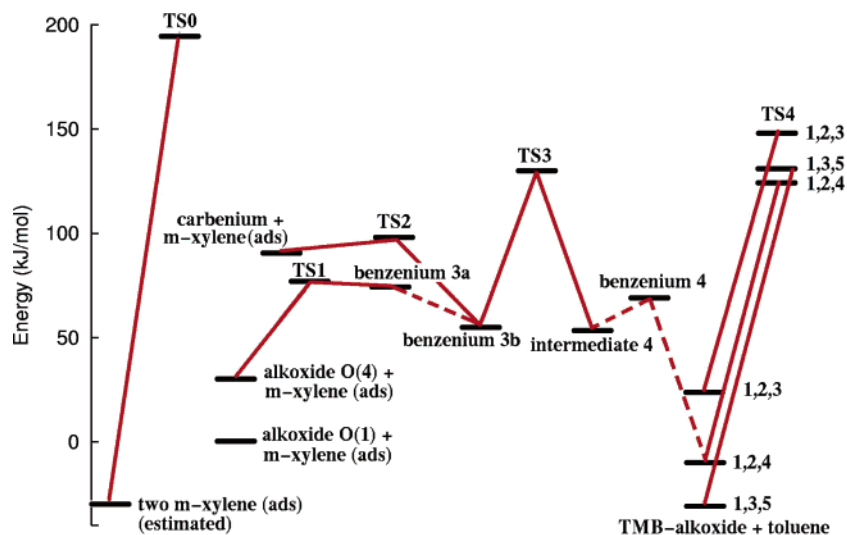
**Figure 8.** Structures at the end of the *m*-xylene disproportionation reaction as shown in Figure 2. See ref 76 for pictures of the structures at the beginning.

Figure 9, and the numerical details are given in Table 4. It is clear that the carbenium ion formation by hydride abstraction (see upper left of Figure 2) is the highest reaction barrier (TS0) with a ZPE-corrected barrier of 206 kJ/mol. However, once a carbenium ion is generated, the catalytic cycle is self-sustaining, avoiding the need for further slow hydride abstraction.

Formation of the bonds that define the trimethylbenzene isomers occurs at TS1 and TS2. The two transition states are

**Figure 9.** Relative potential energy (QM/MM) levels of the diphenylmethane-mediated reactant and transition state structures in the faujasite zeolite. Unless indicated, structures are those applicable to the formation of the 1,2,4 isomer. The highest energy barrier is the formation of the initial alkoxide species (229 kJ/mol, uncorrected). Once the alkoxide is formed, the cycle bypasses this step. Dashed lines indicate a pathway for which a transition state structure has not been located. The energetic placement of the first two structures to the left relative to the remainder has been estimated from calculated single-molecule adsorption energies.

**Table 4.** Relative Potential Energies for the Intermediates and Transition State Structures for the *m*-Xylene Disproportionation Reaction in the FAU Framework as Shown in Figure 9[a]

| state | system energies in kJ/mol | | | | | | |
| --- | --- | --- | --- | --- | --- | --- | --- |
| | QM/MM + ZPE | A[b]-ZPE | QM/MM | QM | MM | $\ln(q/q^*)$[c] | freq (cm$^{-1}$) |
| *m*-xylene (ads.) | 0 | 0 | 0 | 0 | 0 | 0.00 | |
| TS0 | 206 | 16 | 229 | −78 | 307 | −2.99 | 455$i$ |
| alkoxide O(4) + *m*-xylene (ads.) | 30 | 8 | 30 | 19 | 11 | −1.54 | |
| alkoxide O(1) + *m*-xylene (ads.) | 0 | 0 | 0 | 0 | 0 | 0.00 | |
| TS1 | 67 | −17 | 75 | −60 | 135 | 3.24 | 217$i$ |
| benzenium 3a | 68 | −4 | 74 | −61 | 135 | 0.64 | |
| carbenium + *m*-xylene | 82 | −14 | 90 | −91 | 180 | 2.61 | |
| TS2 | 84 | 6 | 93 | −206 | 299 | −1.13 | 324$i$ |
| benzenium 3b | 47 | 19 | 50 | −222 | 272 | −3.60 | |
| TS3 | 113 | 25 | 125 | 53 | 73 | −4.81 | 1112$i$ |
| intermediate 4 | 45 | −6 | 47 | 94 | −47 | 1.12 | |
| benzenium 4 | 60 | −4 | 64 | −204 | 268 | 0.81 | |
| 1,2,3-TMB-alkoxide + toluene | 19 | −6 | 19 | −8 | 26 | 1.03 | |
| 1,2,3-TS4 | 127 | 7 | 143 | −43 | 186 | −1.33 | 46$i$[d] |
| 1,2,4-TMB-alkoxide + toluene | −15 | 1 | −15 | −36 | 20 | −0.35 | |
| 1,2,4-TS4 | 104 | −1 | 120 | −58 | 177 | 0.27 | 18$i$ |
| 1,3,5-TMB-alkoxide + toluene | −34 | 13 | −35 | −42 | 7 | −2.46 | |
| 1,3,5-TS4 | 111 | −20 | 126 | −52 | 178 | 3.79 | 128$i$ |

[a] Potential energies are broken into QM and MM contributions, and temperature-dependent entropic effects are calculated from the harmonic approximation at 623 K. The first two structures are missing a spectator *m*-xylene relative to the other structures. See Table 3 for reference structure information. [b] Vibrational Helmholtz free energies (A) are calculated from the harmonic partition function and include the ZPE contribution. [c] The ratio of state (*q*) to reference state (*q**) partition functions does not include the ZPE contribution. [d] There is a second imaginary frequency of 12$i$ cm$^{-1}$ which is taken to be zero in the vibrational calculations. Repeated attempts to converge this structure to a first-order saddle point were unsuccessful, apparently due to the flat potential energy surface.

distinguished by the carbenium species state of binding. At TS2, the carbenium is free to react with another *m*-xylene anywhere in the supercage. Localization of the TS2 transition state structures for the various isomers (without a zeolite portion in cluster) suggests that the barriers are similar for the 1,2,4 and 1,3,5 isomers and about 15 kJ/mol higher for the 1,2,3 isomer. At TS1, the active species is bound to the acid site as an alkoxide.[76] At first glance, it might seem that the relative barriers at these steps for the three isomers would determine the local product selectivity. However, the molecules must cross significantly higher barriers (TS3 and TS4) in the supercage before forming the products. It can therefore be reasonably assumed that the TS1 and TS2 steps will be recrossed many times, likely along different isomeric pathways. The supercage of the FAU

framework can thus be viewed as a mixing pot, producing an equilibrium distribution of isomers before they undergo hydride transfer to give the product TMB isomers.

The activation energy barriers for the diphenylmethane-mediated pathway are similar to those for the simpler methoxide-mediated pathway. The highest barriers in the closed cycle occur at the final hydride transfer step (TS4). The ZPE-corrected potential energy barriers for formation of the three isomers are 109 (1,2,3), 119 (1,2,4), and 145 (1,3,5) kJ/mol, indicating that, without entropic corrections, the lop-sided 1,2,3 isomer is favored. Comparison of these barrier heights to those for the methoxide-mediated pathway indicates that, even in the wide-pore FAU framework, there may be a preference for the methoxide-mediated pathway. With vibrational free energy

corrections, the barriers are 121 (1,2,3), 116 (1,2,4), and 112 (1,3,5) kJ/mol. Thus, incorporation of entropic effects through the harmonic approximation results in a reverse in the qualitative ordering of the isomer transitions states to favor the 1,3,5 isomer. The reversal is made possible by complementary shifts in both the reactant and transition state corrections.

Comparison to previous computational studies is possible. Blaszkowski et al.[46] studied the toluene disproportionation pathway and found consistently higher activation energies for each step. As with the methoxide-mediated pathway, the higher activation energies are likely due to the small cluster size and the lesser degree of aromatic substitution. Rozanska et al. also used cluster calculations[47] and periodic calculations in MOR[94] to study the toluene to benzene methyl transfer reaction with similar results.

**3.3. Comparison to Experiment.** Results for the two pathways are in general agreement with experiment. Corma et al. derived intrinsic activation energies between 85 and 119 kJ/mol from their kinetic data.[59] Our ZPE-corrected rate-limiting potential energy barriers are 136 kJ/mol for the methoxide-mediated pathway (TS6) and 109 to 145 kJ/mol for the diphenylmethane-mediated pathway (TS4). Vibrational free energy corrections change the methoxide-mediated pathway to 135 kJ/mol and the diphenylmethane-mediated pathway range to 112−121 kJ/mol. Relative activation energy comparison can be made between the two pathways because both scales use a state with adsorbed *m*-xylene as the reference. Our calculated estimates are thus on the high end of the experimental range, corresponding well to their less-dealuminated catalysts.

Because the experimental selectivities are likely masked by product shape selectivity phenomenon and surface reactions, it is difficult to compare selectivities with experiment. The experimental selectivities to the 1,2,3 and 1,2,4 isomers given in Table 1 differ by a factor of 10. At a typical test reaction temperature (623 K), such an order of magnitude difference in rate constants can be achieved with a difference in activation energy barriers of 12 kJ/mol. We see this degree of variation in our activation energy barriers (see Tables 2 and 4), but the relative activation energies, irrespective of corrections, do not coincide with the published experimental selectivities. Therefore we conclude that the local reaction characteristics calculated here are significantly different from those probed by experiments that rely on monitoring of external products.

An estimate for the relative abundance of the three trimethyl-benzenes *inside the pores* from MAS NMR also suggests that the 1,2,3 and 1,2,4 isomers are favored.[42] Even though the studied reaction, methanol to gasoline over HZSM-5, was different, it may still be comparable because there are indications that it also proceeds through an equilibrium distribution of highly methylated aromatics in both HZSM-5[95] and HBEA.[96] In good agreement, and irrespective of vibrational free energy corrections, our results predict that the 1,3,5 isomer will be similarly disfavored for the methoxide-mediated pathway. The results for the diphenylmethane-mediated pathway are similar but only without the first-order free energy corrections.

## 4. Conclusions

Computational examination of the diphenylmethane-mediated and methoxide-mediated disproportionation of *m*-xylene has allowed us to elucidate the controversial transition state shape selectivity phenomenon. Without first-order entropic corrections, both pathways favor the 1,2,4 and 1,2,3 TMB isomers over the 1,3,5 isomer. However, the preference for the 1,2,4 isomer over the 1,2,3 isomer varies across pathways and frameworks and is sensitive to inclusion of entropic contributions. For the methoxide-mediated pathway, activation energy shifts capable of producing significant selectivity shifts are seen across frameworks. Additionally, a change of isomer preferences is seen in the MFI framework when entropic effects are included. These environmental shape effects indicate that transition state shape selectivity is present in this reaction.

The relative contribution of each pathway to the overall reaction rate is important in determining observable transition state shape selectivity. Our ZPE-corrected rate-limiting potential energy barriers for the methoxide-mediated pathway (136 kJ/mol) falls within the range of barriers for the diphenylmethane-mediated pathway (109 to 145 kJ/mol). When the barrier heights are corrected using first-order entropic effects from the harmonic approximation, the rate-limiting step (methoxide formation) in the methoxide-mediated pathway has an activation free energy barrier of 135 kJ/mol compared to the rate-limiting hydride transfer step in the diphenylmethane-mediated pathway which has barriers between 112 and 121 kJ/mol. Though relative rates are sensitive to small activation energy differences, uncertainties in the accuracy of the calculations and in examination of only a single active site limit the predictive power. The relative activation energies suggest that both pathways will be populated but that the diphenylmethane-mediated pathway dominates in FAU. The methoxide-mediated pathway may be expected to be more favorable in the more restricted zeolites.

For the methoxide-mediated pathway, comparison across the FAU, MOR, and MFI zeolite pore types provides direct information on how the pore shape affects the selectivity-determining transition state structures. The placement of the transferring methoxide and the *m*-xylene molecule differ greatly while maintaining similar critical bond lengths. Pore geometry shifts but does not change the relative potential energy ordering of the transition states. A first approximation for the entropic effects at the transition state is available through the harmonic approximation and the second derivatives. Entropic corrections to the relative barrier height can be significant (−3 to 26 kJ/mol) and, in the MFI framework, result in a selectivity shift from the 1,2,4 to the 1,2,3 isomer. There appears to be some correlation between framework and curvature of the potential energy surface along the reaction coordinate. In the most open FAU framework, the curvature is smallest.

Electronic characteristics at the various aromatic substitution positions likely determine a minimum transition state potential energy for a given isomer.[18,68,97−100] This single-point energy or barrier will be achievable if there is sufficient spatial freedom

(94) Rozanska, X.; Van Santen, R. A.; Hutschka, F. *J. Phys. Chem. B* **2002**, *106*, 4652−4657.
(95) Song, W.; Haw, J. F.; Nicholas, J. B.; Heneghan, C. S. *J. Am. Chem. Soc.* **2000**, *122*, 10726−10727.
(96) Sassi, A.; Wildman, M. A.; Ahn, H. J.; Prasad, P.; Nicholas, J. B.; Haw, J. F. *J. Phys. Chem. B* **2002**, *106*, 2294−2303.

(97) Korchowiec, J.; Nalewajski, R. F. *Int. J. Quantum Chem.* **1992**, *44*, 1027−1040.
(98) Corma, A.; Zicovich-Wilson, C. *J. Phys. Org. Chem.* **1994**, *7*, 364−370.
(99) Langenaeker, W.; De Proft, F.; Geerlings, P. *J. Phys. Chem.* **1995**, *99*, 6424−6431.
(100) Song, C.; Ma, X.; Schmitz, A. D.; Schobert, H. H. *Appl. Catal.* **1999**, *182*, 175−181.

in the reaction cavity. Entropic effects may then further modify the energetics based on the relative freedom available to the reactants or transition state structures. The resulting shifts in the selectivity due to environmental shape effects are thus a composite of potential energy and entropic effects.

Examination of the diphenylmethane-mediated pathway yields a number of useful observations pertaining to the affects of local pore geometry. More specifically, it calls into question the generality of the original definition of *restricted* transition state shape selectivity. We have already seen that simply turning on and off pathways, as proposed in the original definition, is unnecessarily limiting. A new view is needed that encompasses all the effects that local pore shape may have on relative transition state energies and therefore selectivities. In this case, the steps where the isomer-defining bonds are formed are not those that limit the rate of reaction. They occur before the rate-limiting step(s) and should therefore result in formation of a local equilibrium distribution of intermediates. This means that environmental shape contributions across a wider region of transition states in the pathway must be accounted for in any definition. With this in mind, we propose to define the general term "transition state shape selectivity" as *any local shift in relative rates of isomer formation due to environmental shape-induced changes in energetics at the reaction dividing surfaces.* Here "local" is taken to mean within a few molecular lengths of the active site. The restriction to *local* selectivity allows product and transition state selectivity to be both operative and yet separable in a given reaction. Anderson et al.'s "active site shape selectivity"[42] would also be encompassed by this general definition.

The potential energy surface schematic for the diphenyl-methane-mediated reaction also hints at how relative intermediate energies could be affected by pore shape. If there were no differences between the energetics of the TS4 (see Figure 9) transition states, then it would be the relative energies of the TMB-alkoxides that determined their population and therefore local selectivity. This is apparently identical to the "inverse shape selectivity" proposed by Santilli et al. when they found they could relate product selectivity to fit and therefore population of intermediates inside the pores.[43] To put this phenomenon in the same context of potential energy surfaces as transition state shape selectivity, yet distinguish it, we suggest that it be called "intermediate shape selectivity".

From a design perspective, a valuable lesson concerning the possibilities of reaction control through environmental shape

modification has been learned. It is clear that there is a molecular bulkiness regime where transition states to all product isomers are accessible yet where relative barrier heights can be shifted. The magnitude of the achievable shifts appear to be in the 10−20 kJ/mol range (see Table 4 and Figure 6). The same trend can be seen in the comparison of the relative methylation barrier spreads. For toluene methylation on an environment-free zeolite cluster, the spread between barriers to the isomers is only 7 kJ/mol.[46] With inclusion of the full MOR environment, the spread becomes 15 kJ/mol.[17] Finally, in this work, the spread for the bulkier *m*-xylene methylation in MOR is 31 kJ/mol.

Two important future directions of research into transition state shape selectivity can be foreseen. First, there must be computational methods that are capable of efficiently predicting such effects. Methods capable of examining the effects across the entire dividing surface or transition state ensemble will be especially important since it is clear from this work that even first-order entropic effects at the transition state can play a significant role. Second, ideas for increasing the magnitude of the effect should be developed and demonstrated. Prospects for completely excluding formation of one transition state, as in the original concept of *restricted* transition state selectivity, should be pursued. Increases in specific binding and active site homogeneity are expected to be beneficial because they will improve control. Strategies for minimizing product shape selective effects such as avoiding substantial diffusion distances will also be important. Insights can also be expected from enzyme and homogeneous chiral catalysis and especially in conjunction with computational modeling.

**Supporting Information Available:** Complete sets of atomic point charges for the hydrocarbon species (PDF). Structures and absolute energies for all stationary points (TXT). This material is available free of charge via the Internet at http://pubs.acs.org.

JA0381712